LA-UR-17-29185
Approved for public release; distribution is unlimited.

Title: Quantifying the stress fields due to a delta-hydride precipitate in alpha-Zr matrix

Author(s): Tummala, Hareesh
Capolungo, Laurent
Tome, Carlos

Intended for: Report

Issued: 2017-10-19 (rev.1)

Quantifying the stress fields due to a δ-hydride precipitate in α-Zr matrix

Hareesh Tummala, Laurent Capolungo, Carlos N. Tomé

MST Division, Los Alamos National Laboratory Los Alamos, NM 87545

This Report addresses the Milestone M2MS-17LA0201031: "Issue Summary Report on Hydride Effects during Storage of UO2 Fuel"

Abstract

This report is a preliminary study on δ-hydride precipitate in zirconium alloy performed using 3D discrete dislocation dynamics simulations. The ability of dislocations in modifying the largely anisotropic stress fields developed by the hydride particle in a matrix phase is addressed for a specific dimension of the hydride. The influential role of probable dislocation nucleation at the hydride-matrix interface is reported. Dislocation nucleation around a hydride was found to decrease the shear stress (S_{13}) and also increase the normal stresses inside the hydride. We derive conclusions on the formation of stacks of hydrides in zirconium alloys. The contribution of mechanical fields due to dislocations was found to have a non-negligible effect on such process.

---

1. Introduction

Zirconium (Zr) alloys have been extensively used in the nuclear industry as *clad* for nuclear fuel in Light Water Reactors (LWR) and as *pressure tubes* in Heavy Water Reactors (HWR) [23]. A good compromise of mechanical (e.g. high strength, ductility), chemical (e.g. excellent corrosion resistance) and nuclear (low absorption cross-section of thermal neutrons) properties made use of these alloys possible for the most challenging applications in nuclear reactors.

However, Zr alloys show a significant affinity for absorbing hydrogen during manufacturing and operation. Due to the lower hydrogen solubility level at elevated temperatures, the absorbed hydrogen in the alloy precipitates to form zirconium hydrides [14]. These hydride precipitates have been identified as the cause for the degradation of mechanical properties (e.g. ductility, fracture toughness) of Zr alloy. Hydrides are thought to precipitate at defects and grain boundaries due to the tendency of hydrogen to diffuse down the thermal and concentration gradients, and up the hydrostatic stress gradients [3]. In fact, formation and growth of these brittle hydrides at regions of high stress concentration (e.g. crack tips) in Zr alloys leads to a time-dependent failure mechanism, known as *Delayed Hydride Cracking (DHC)* [23]. Hydride precipitates are preferentially aligned along the circumferential direction of the clad tube as a combined consequence of texture, the internal stress applied by swelling fuel, and the coolant pressure. During their transfer to dry storage, due to the thermal fluctuations, hydrides re-dissolve into the Zr alloy clad and re-precipitate along the radial direction. The radial alignment of the hydrides is due to the changes in stress state of the clad caused by the absence of the coolant. This *stress-induced re-orientation* is undesirable as the

radially oriented precipitates act as stress concentrators and may lead to fracture of the clad during long-term storage [20]. It is still unclear how these complex stress interactions among hydrides influence their arrangement and in-turn, the overall mechanical performance of the Zr alloy clad. In this report, we aim at throwing some light on this question.

This study aims at quantifying the contribution of mechanical stress fields and their evolution on the self-organization of hydrides (stacking). Further, it aims at quantifying the stress state near and within the hydride. This report is organized as follows. Section 2 provides an overview of experimental results on the morphology and orientation of the hydrides in Zr alloys. Details of the simulation setup and material constants used in the current study are presented in Section 3. Simulation results on a hydride in Zr matrix with and without dislocations in the simulation volume are presented in Section 4, where results indicate that there is no plastic relaxation around a hydride. However, the nucleating dislocations at the interface were observed to alter the mechanical fields in and around the hydride. Final conclusions are presented as the effective shielding distance, defined as the minimum distance below which the probability of nucleating another hydride close-by is zero, around the hydride of specific dimension.

2. Experimental evidence of hydride stacks in zirconium

In one of the earliest reviews published on hydride precipitates in Zr alloys, the dependence of embrittlement on *morphology* and the *orientation of the hydride* relative to the matrix was highlighted [17]. Single hydrides take the shape of either needles or platelets depending on cooling rate and availability of hydrogen [17]. The strain energy density was observed to be lowest for disc/platelet morphologies [16]. Except in special cases, hydrides in Zr alloys were always observed to arrange in stacks. These stacks of hydrides, which are generally referred to as 'macroscopic hydrides', have no reason to show similarities in morphology and orientation with that of single hydride platelets or 'microscopic hydrides'. The macroscopic morphology and orientation would in-fact depend on the local arrangement and stress fields of these microscopic hydrides. The scanning electron microscopy (SEM) observations of a stress-relieved annealed (SRA) zircaloy showed two morphologies of microscopic hydrides: one close to 'equiaxed' (short and thick hydrides) and another 'elongated'.

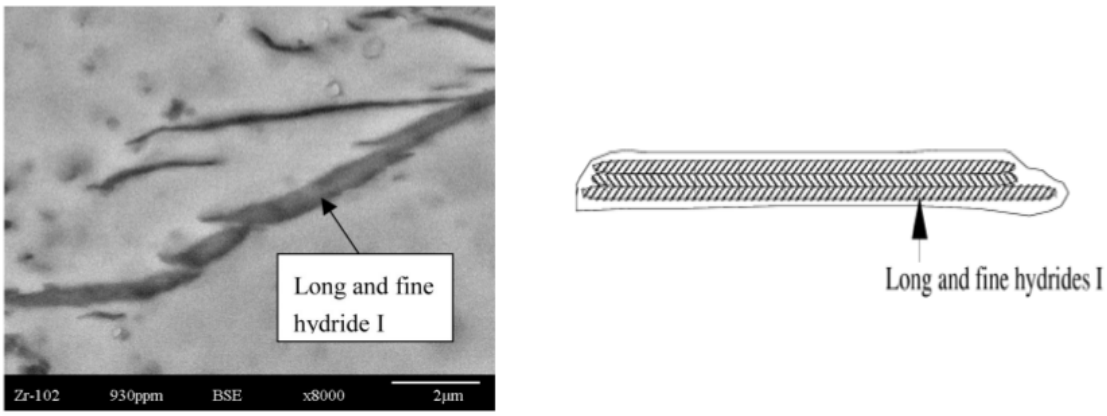

Fig. 1. (a) SEM image and (b) Schematic of the “Long and fine hydrides I” [2]

Concerning the arrangement of these microscopic hydrides, three different macroscopic hydride configurations were reported [2]. The first configuration, referred by the author as "long and fine hydride I", had the elongated microscopic and the macroscopic hydrides in the same orientation. The elongated microscopic hydrides were arranged in parallel as shown in Fig. 1. This configuration was the most frequently found in SRA Zircaloy used by the author.

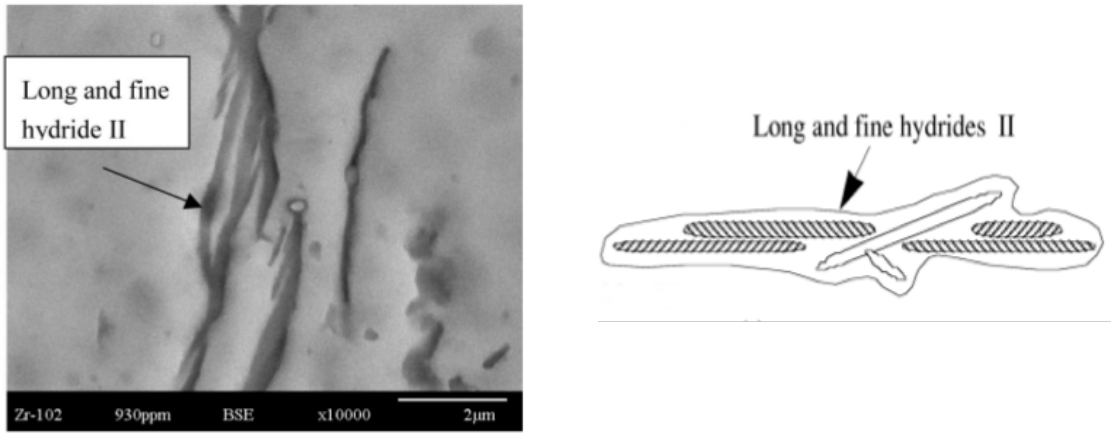

Fig. 2. (a) SEM image and (b) Schematic of the "Long and fine hydrides II" [2]

The second macroscopic hydride configuration, referred to as "long and fine hydride II", had a more complex structure with elongated microscopic hydrides and the macroscopic hydride in different orientations. The arrangement had few elongated hydride platelets of same orientations stacked together which were separated at a distance from the other local stacks as shown in Fig. 2.

Finally, the third configuration, referred to as "Long and fine hydride III", had few equiaxed microscopic hydrides stacked together and had different orientation than the macroscopic hydride. The microscopic hydrides were spaced as shown in Fig 3.

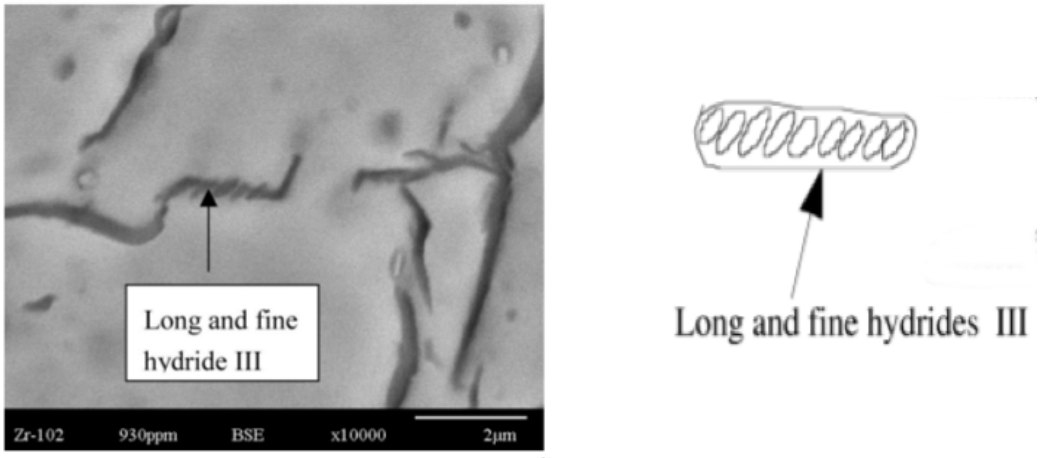

Fig. 3. (a) SEM image and (b) Schematic of the "Long and fine hydrides III" [2]

Even if this is not the complete catalog of the different configurations of macroscopic hydrides, these SEM observations give us an idea about the different configurations into which these complex hydrides can segregate. A different study by Singh et al. also reported a two-

level organization of hydrides in Zr alloy [24] highlighting the importance of understanding the organization in macroscopic hydride stacks and their relationship to hydride embrittlement.

An aspect which may influence the hydride orientation in Zr alloy is the plastic deformation around it. Extreme brittleness of the hydride phase could be the result of the influence of the hydrogen lattice on the movement of glide dislocations in the Zr matrix [5]. The high strain field induced by hydride formation is expected to cause plastic relaxation and high dislocation density around the hydride. Sometimes, a large strain field associated with the small hydrides makes it difficult to reveal the dislocations generated closest to the hydride's interface [23]. Dislocations formed around a hydride only partially relieves the dilatational misfit strain of the hydride in Zr matrix [10]. Dislocations generated around the hydride precipitates were in the form of loops attached to the ends of the needles with <11-20> Burgers vector lying on or near the basal plane (see Fig. 4). It is still unclear on whether these dislocation loops observed around hydride precipitates were due to plastic relaxation of the dislocations around the hydride or due to dislocation nucleation near the matrix-hydride interface. In any case, the dislocations generated at the interface will change the strain field around the hydride and may play a role in hydride stack arrangement.

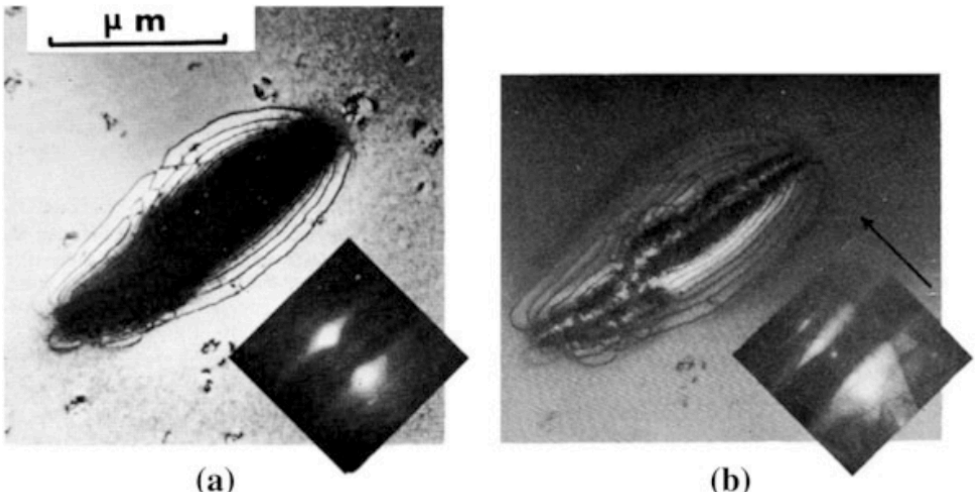

Fig. 4. (a) Dislocation loops around a microscopic hydride [11]; (b) Dislocation loops around a macroscopic hydride [11]

3. Simulation procedure

In this work, a Fast Fourier Transform based 3D Discrete Dislocation Dynamics (DDD-FFT) simulation technique [7] is used to solve the complex mechanical fields generated by a second phase material (δ-hydride in Zr matrix) in the presence of dislocations in the simulation volume.

The influence of a *δ-hydride* in α-Zr is studied for three different cases. In the first (elastic) case, the mechanical fields due to a *δ-hydride* in the absence of dislocations in the α-Zr matrix is analyzed. This is followed by a 'relaxation' case, where the *δ-hydride* transformation takes place in the presence of dislocations in the α-Zr matrix. Finally, in the third ('nucleation') case, the influence on the mechanical fields due to dislocation nucleation close to a *δ-hydride* are discussed in the presence of dislocation in the α-Zr matrix. In every

case, relaxation simulations were performed considering only the eigenstrain corresponding to the hydride (no external applied load).

The simulations setup used and material parameters considered in the current study are presented in this section. Simulations were carried out in a periodic volume with cube side of $2\mu m$. An ellipsoid-shaped δ-hydride of dimensions $100nm$ x $300nm$ x $30nm$ was placed at the center of the cubic α-Zr single crystal, see Fig. 5. The dimension of the δ-hydride is within the range of the hydride dimensions found in experiments [13].

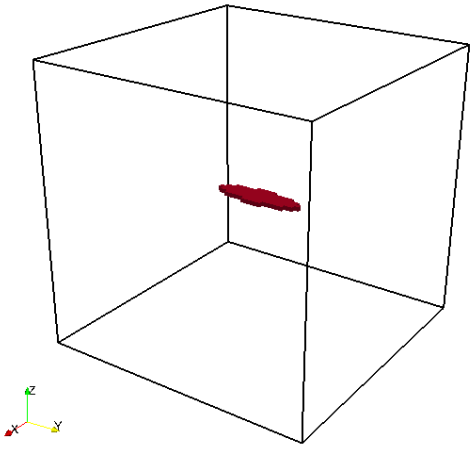

Fig. 5. A δ-hydride centered in α-Zr matrix

3.1. Orientation of the hydride in Zr matrix

The hydride was placed on the basal plane of the α-Zr matrix, and such that the [11-20] direction aligns with the long axis of the δ-hydride. Fig. 6 shows the directions of the oriented matrix and the alignment of the hydride in the simulation volume. It should be noted that the δ-hydride itself was considered elastic (no plastic deformation inside the hydride).

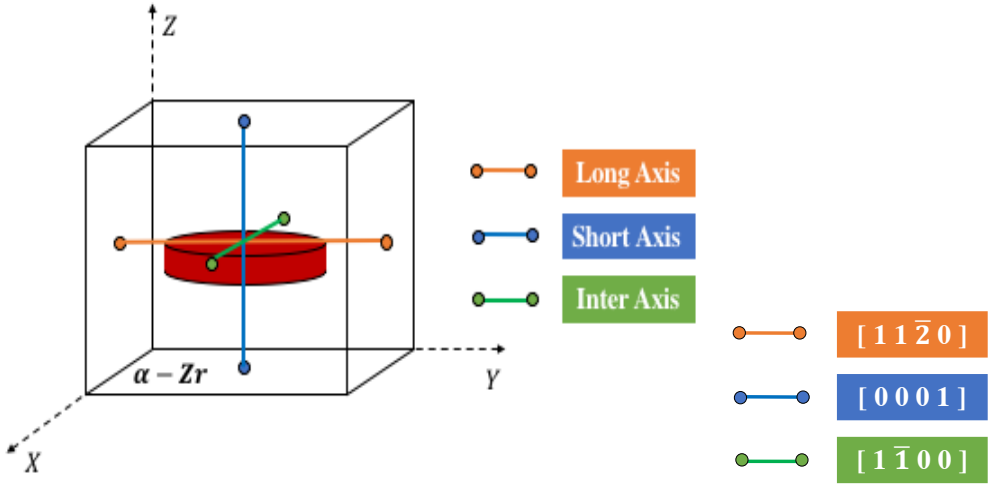

Fig. 6. Schematic of a δ-hydride with its long axis oriented along [11-20] direction of α-Zr matrix

3.2. Material parameters of Zr and δ-hydride

The lattice constants (in Å) and anisotropic elastic constants (in MPa) of a Zr single crystal exhibit a significant dependence on temperature [19]. Considering that a nuclear reactor operates at about 573K, material constants of α-Zr were considered at 573K (see Table 1). But, due to the lack of experimental data on anisotropic elastic constants of δ-hydride at 573K, elastic constants (in MPa) of the δ-hydride at 0K (see Table 1) were used here from the results of DFT simulations [22].

Material parameters	α-Zr (HCP)	*δ-hydride* (FCC)
a	3.23	4.78
c	5.147	-
C_{11}	155400	63000
C_{33}	172500	65000
C_{44}	36300	93000
C_{66}	36300	101000
C_{12}	67200	28000
C_{13}	64600	44000

Table 1. Material parameters of α-Zr at 573K and *δ-hydride* at 0K

In Zr, prismatic slip is found to be the easiest slip, much more than basal and pyramidal slip [8]. This is due to the huge differences in friction stresses associated with basal, prism and pyramidal systems. The friction stresses (in MPa) [1] chosen for different systems in the present simulation are presented in Table 2.

Slip modes in α-Zr	Lattice friction (in MPa)
Basal	179.41
Prismatic	6.67
$Pyramidal < a >$	76.0
$Pyramidal < c + a >$	76.0

Table 2. Lattice friction stresses for Zr at 573K

3.3. Stress-free transformation strain of δ-hydride

Eigen strains are known to govern the strain energy associated with the accommodation of hydrides in a Zr matrix [23]. Linear and volumetric misfit strains associated with the formation of zirconium hydrides valid over a temperature and composition range were recently reported [24]. Temperature dependence of atomic radii and volume valid over a temperature and composition range changes the misfit strain computed using the atomic radii data. The variation with temperature of misfit strains for zirconium hydrides is given by:

$$\epsilon_{11} = 0.03888 + 2.315 \times 10^{-5}\mathrm{T}$$

$$\epsilon_{22} = 0.06646 + 1.9348 \times 10^{-5}\mathrm{T}$$

The Eigen strain tensor $\boldsymbol{\epsilon}^{eigen}$ calculated at 573K is

$$\boldsymbol{\epsilon}^{eigen} = \begin{bmatrix} 0.0521 & 0.0 & 0.0 \\ 0.0 & 0.0521 & 0.0 \\ 0.0 & 0.0 & 0.0722 \end{bmatrix}$$

where 5.21% is the misfit strain normal to hydride platelet (short and intermediate axis represented in Fig. 4); 7.22% is the misfit strain along the hydride platelet (long axis).

3.4. Initial dislocation network

In order to start with a more realistic dislocation microstructure, a relaxation test was performed with randomly distributed dislocation loops on different slip systems in the simulation volume. In the first step, a dislocation configuration with loops randomly distributed is loaded with a randomly chosen initial stress tensor and at a randomly chosen increment rate for 1000 simulation steps. The time step was chosen such that it still allows interaction among dislocations. After the loading stage, the relaxation stage is initiated by abruptly removing the externally applied load on the simulation volume and allowing the dislocations to glide under their own stress field. The relaxation stage is stopped when the dislocation density does not evolve for more than 100 consecutive steps (i.e., no considerable plastic strain is accumulated by dislocations under their own stress field) and the dislocation microstructure is extracted. Such a relaxed dislocation configuration is chosen as the *initial dislocation microstructure* during the simulations. In the present study, four different initial distribution of dislocation loops were considered to generate relaxed microstructure with different final dislocation density. Different relaxed dislocation microstructures are hereby referred as MIC_B1, MIC_B2, MIC_P1 and MIC_P2. 'MIC' is given as an abbreviation to the dislocation microstructure, B and P referring to the highest density on the Basal and Prismatic systems, respectively.

Fig. 7.a and 7.b show the initial dislocation configuration of total density ρ_{total}=1.1 10^{13}m^{-2} with dislocation loops distributed on different slip systems and the final relaxed configuration of total density ρ_{total}=1.2 10^{13}m^{-2} with complex dislocation networks.

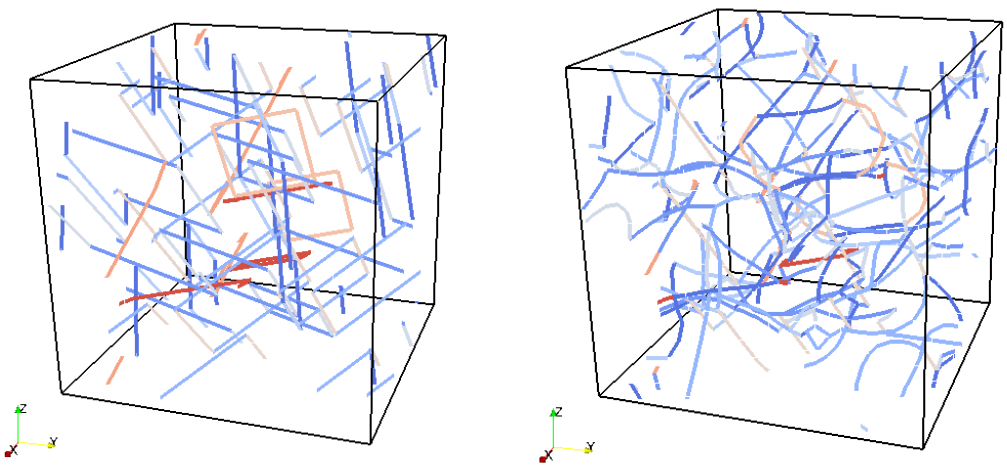

Fig. 7. (a) Initial dislocation configuration with randomly distributed dislocation loops; (b) Relaxed dislocation configuration, MIC_B1 with complex dislocation networks

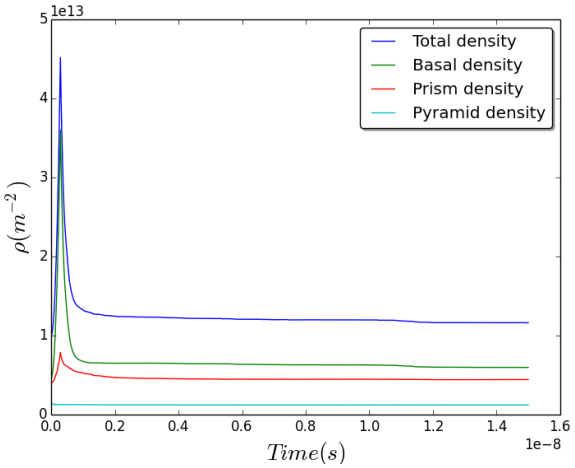

Fig. 8. Dislocation density evolution during relaxed dislocation microstructure, MIC_B1 generation.

To study the influence of pre-existing Basal or Prismatic dislocations on the stress fields in and around the hydride, we considered different Basal and Prism densities. In addition to the variation in the total dislocation density shown in Fig. 8 and Fig. 9, the individual dislocation densities on the Basal and Prismatic planes are also reported.

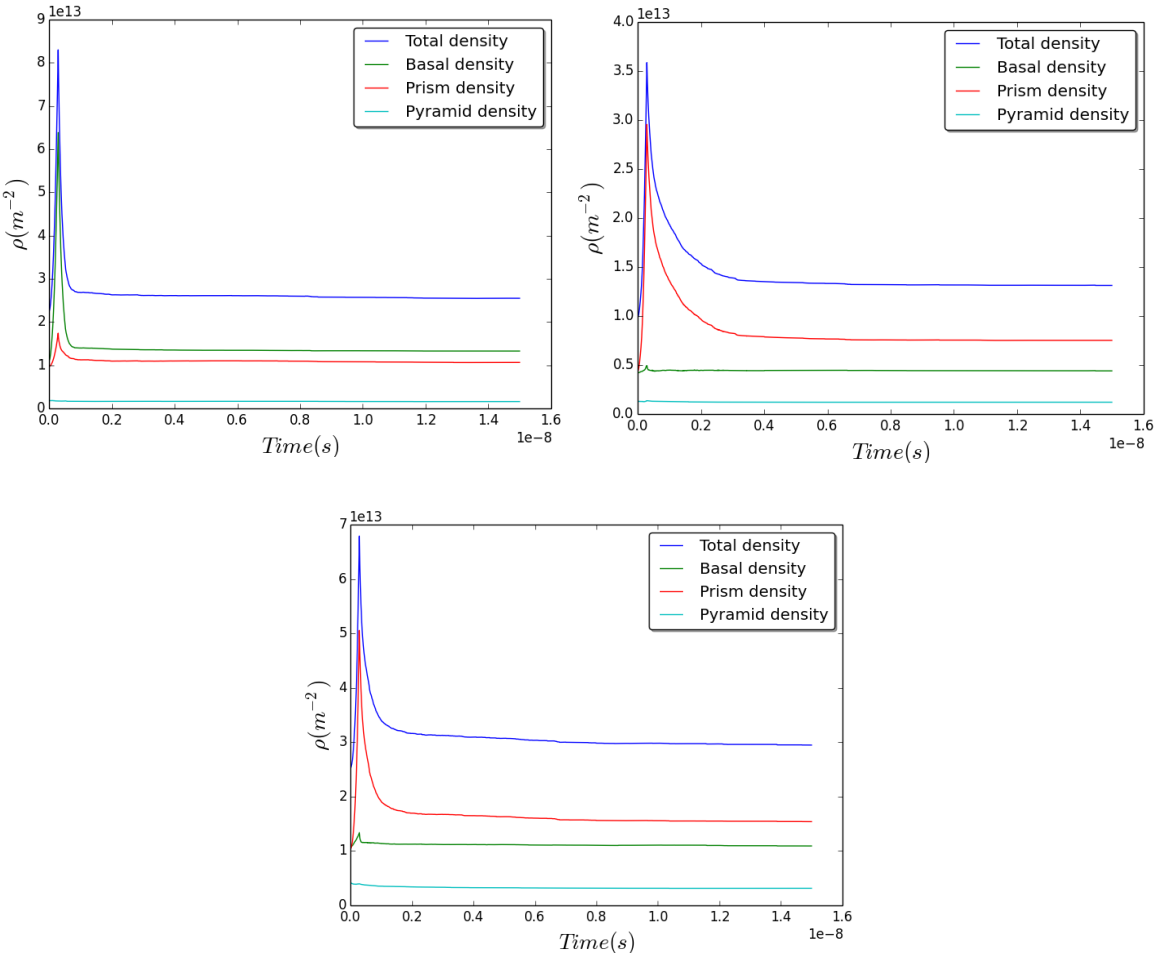

Fig. 9. Dislocation density evolution during relaxed dislocation microstructure generation in MIC_B2 and MIC_P1 and MIC_P2 respectively

4. Results and discussion

4.1. *CASE-I: Elastic stresses due a δ-hydride in α-Zr*

A δ-hydride with high eigenstrain, ϵ^{eigen} as reported in Section 3.3, is placed in the α-Zr matrix in the absence of any dislocations. The elastic stress fields generated in the α-Zr matrix due to the δ-hydride are presented here. The stress fields were computed on a slice positioned at the center of the simulation volume with the normal parallel to X-axis. Further, the results are reported in the range of stress -250 MPa to 250 MPa to show uniformity while comparing results from different simulations.

The S_{33} components of the stress field shown in Fig. 8 indicates that the α-Zr matrix is in tension corresponding to the direction in which the hydride has the highest eigenstrain. This result can be understood as a combined effect: while ε_{33} will induce compression along the *Z*-axis, the Poisson effect associated with ε_{11} and ε_{22} will induce tension along *Z*-axis. The normal stress (S_{33}) and shear stress (S_{13}) were observed to be uniform inside the hydride. These results are in agreement with the famous work of Eshelby [25].

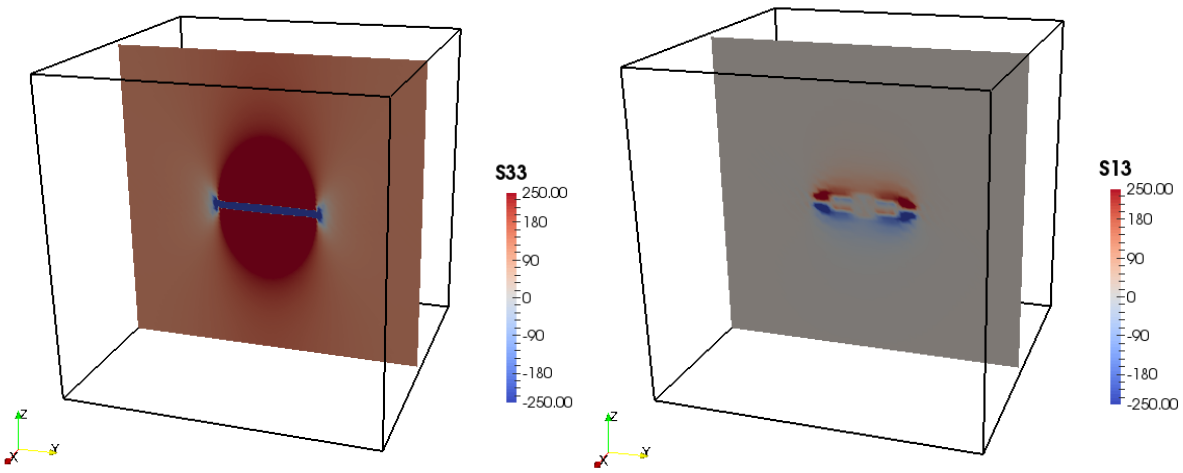

Fig. 8. S_{33} and S_{13} components of the elastic stress field due to the presence of a δ-hydride in α-Zr matrix with no dislocations

4.2. *CASE-II: Plastic relaxation around a δ-hydride in α-Zr matrix*

In order to understand the influential role of dislocations on the mechanical fields due to a δ-hydride in the α-Zr matrix, relaxation simulations were performed with different initial microstructures (see Section. 3.4).

A δ-hydride is now placed in the presence of different initial dislocation microstructures in α-Zr matrix. Fig. 9 shows the initial setup with δ-hydride and dislocation microstructures MIC_B2 and MIC_P1 used here. Dislocation density evolution during the precipitate transformation, shown in Fig.10, does not show any change with respect to the initial relaxed configuration of Fig 7. This indicates that the stress field of the δ-hydride has no appreciable impact to drive the surrounding dislocations (i.e., no plastic relaxation around the hydride was observed). But, an analysis of the S_{33} component of the stress fields from these simulations (see Fig. 11), shows that the dislocations tend to change the magnitude of the elastic

stress field created by a δ-hydride in the α-Zr matrix. The change in magnitude is directly proportional to the total dislocation density and does not depend on the individual Basal or Prismatic densities.

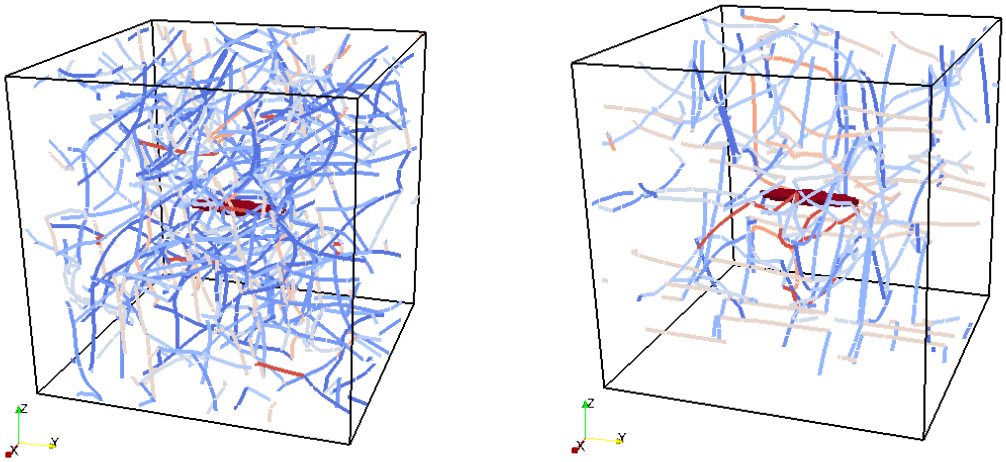

Fig. 9. Initial setup with *δ-hydride* in α-Zr with dislocation configurations, MIC_B2 and MIC_P1, respectively

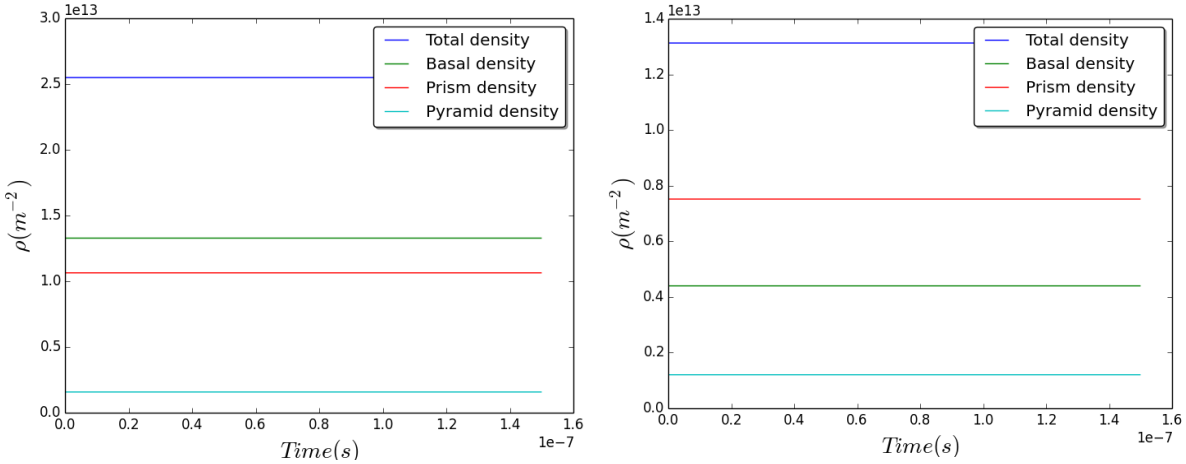

Fig. 10. Dislocation density evolution during precipitate relaxation in the dislocation microstructures MIC_B2 and MIC_P1, respectively.

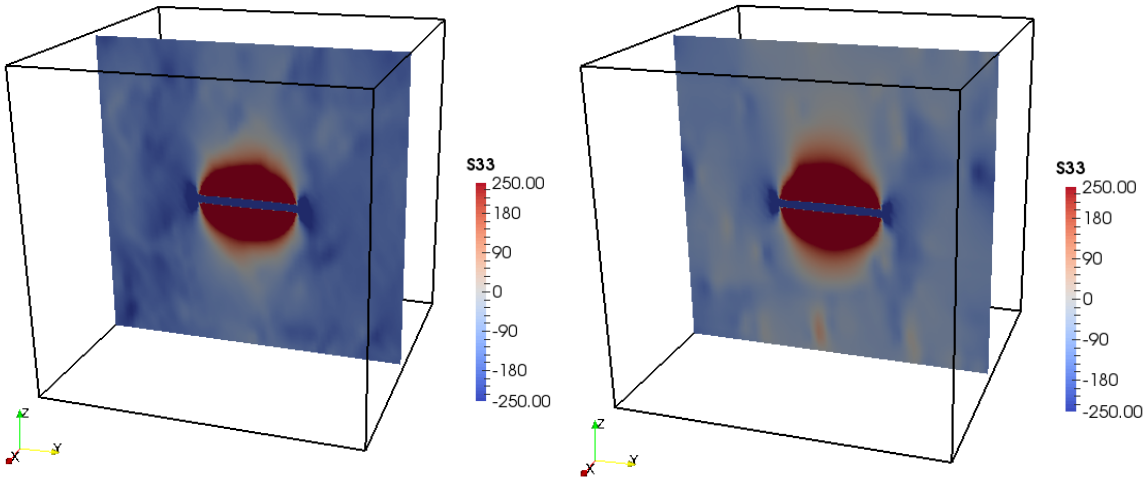

Fig. 11. S_{33} component plotted after precipitate relaxation in the dislocation microstructures MIC_B2 and MIC_P1, respectively.

4.3. CASE-III: Dislocation nucleation from hydride-Zr interface

Dislocation loops were experimentally observed around a hydride in Zr (see Fig. 4). Since, plastic relaxation was not observed from the results in Section. 4.2, there is a definitive need for dislocation nucleation to minimize misfit between hydride and matrix. To study the influence of nucleating dislocations near the interface, a set of dislocation loops were inserted near the matrix-hydride interface. This method was employed to mimic the dislocation nucleation process. The main objective in performing such an analysis is to analyze if the plastic relaxation that was experimentally observed is due to dislocation nucleation around a hydride [11]. The goal here is also to observe the self-organization of nucleating dislocation near the matrix-hydride interface.

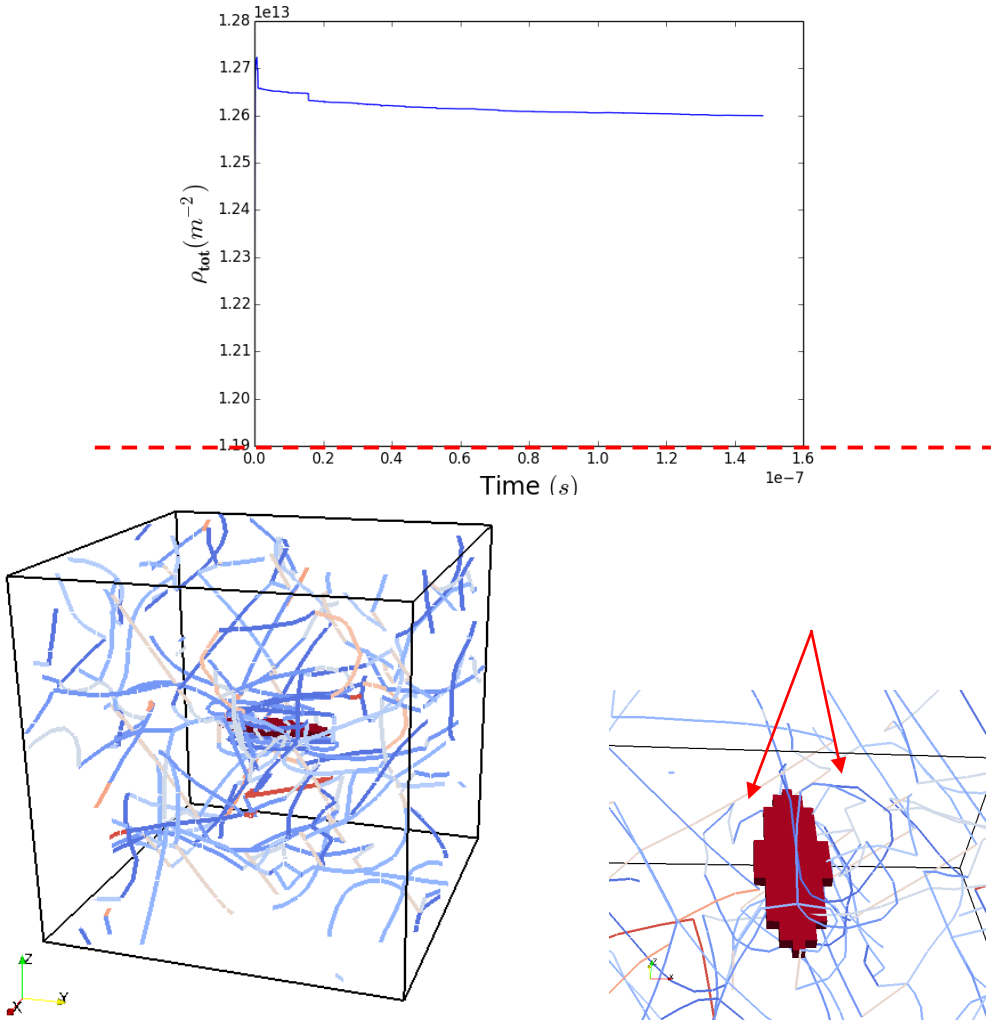

Fig. 12. (a) Dislocation density evolution, with red dash line indicating the initial dislocation density, in the simulation; (b) Snapshot of the final dislocation rearrangement and (c) Top (zoom) view of nucleated dislocations (pointed with red arrows) in simulation MIC_B1

The initial dislocation density during this simulation was ρ_{total}=1.19 10^{13}m^{-2} and is marked with a dash red line in Fig. 12.a. The jump in the dislocation density evolution plot in Fig. 12.a corresponds to dislocation nucleation. Nucleated dislocations were observed to rearrange themselves around the hydride as shown in Fig. 12.b. In the top view (zoom) red arrows point to the nucleated dislocations (Fig. 12.c). Dislocation rearrangement around the hydride in this simulation matches the experimental observation of dislocation around hydrides

in Zr alloys (see Fig. 2.a). Carpenter et al. addressed them as complete dislocation loops around the hydride. The number of dislocation loops surrounding the hydride in the experiments do not match the current observations from the simulations. This discrepancy is due to the limited number of dislocations being used for testing the nucleation process.

4.4. *Influence of dislocation nucleation*

To quantitatively measure the influence of nucleating dislocations around the hydride, true stress values measured on a line drawn along the long axis of the precipitate are compared against the case with no dislocation nucleation. Fig. 13 shows the true stress value drawn on a line along the long axis of the precipitate in the cases with and without dislocation nucleation, respectively.

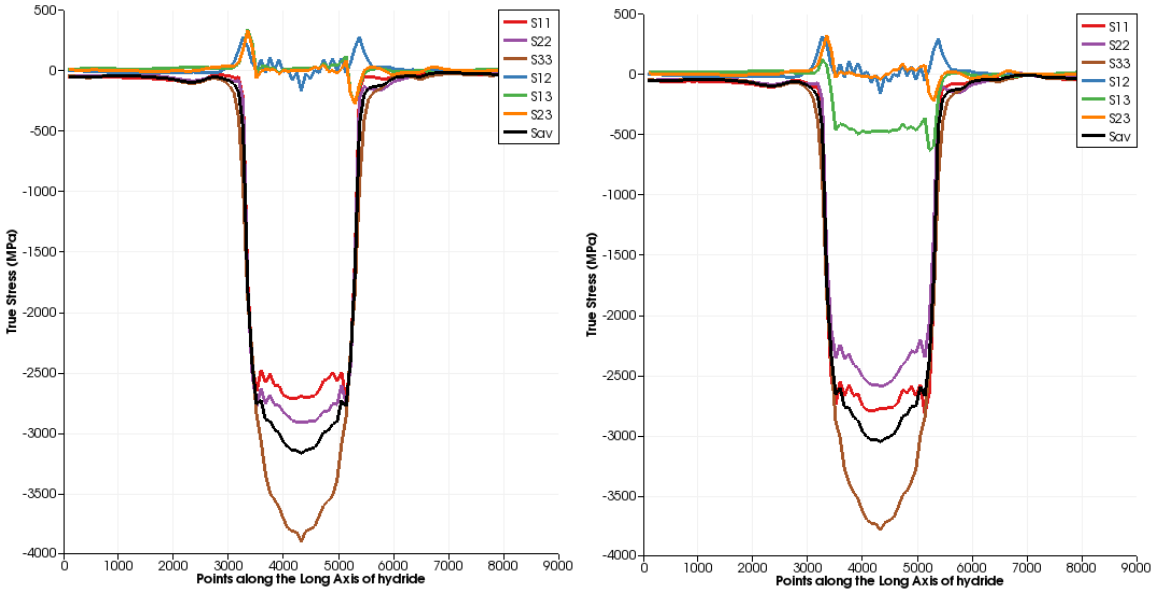

Fig. 13. (a) True stress on a line parallel to long axis for nucleation case; (b) True stress on a line parallel to long axis for no nucleation case in the simulation MIC_B1

The magnitude of the shear stress (S_{13}) decreases by about 500 MPa. Whereas, the normal stresses inside the hydride increases in the range 100-200 MPa. These results indicate that the nucleation of dislocations near the hydride-matrix interface will increase the normal stresses and simultaneously decrease the shear stresses (S_{13} and S_{23}) inside the hydride, thereby influencing the shielding effect of the hydride.

4.5. *Effective shielding distance*

In this section, the spatial position around a hydride where another hydride has the highest probability for nucleation in the Zr matrix is estimated. This is done by computing the dissipation ($E=1/2\sigma_{ij}\epsilon_{ij}^{eigen}$) that would be associated by the formation of a hydride in the stress field induced by the central one. In Fig. 14, the dissipation for the elastic case, relaxation and nucleation cases near the precipitate interface are compared.

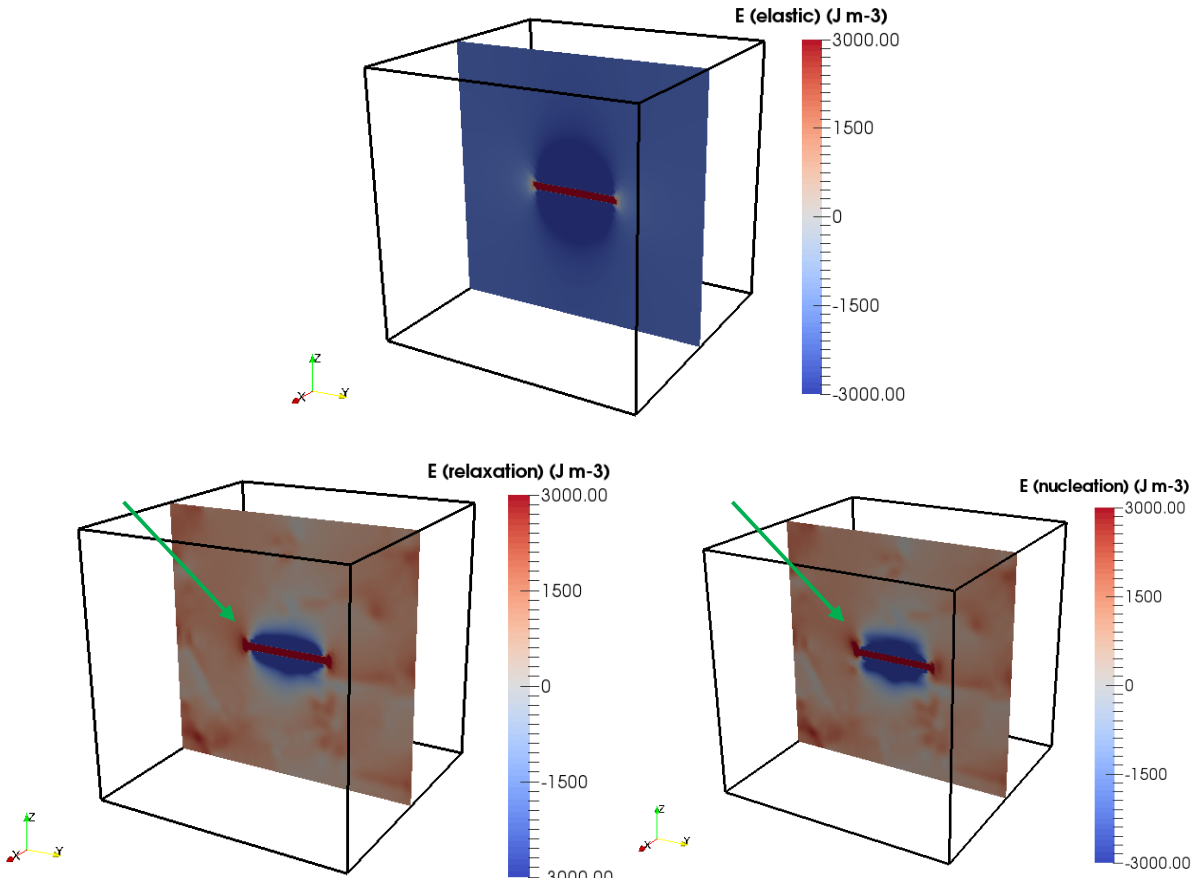

Fig. 14. (a) Dissipation for elastic case; (b) Dissipation for the case with dislocations but no nucleation; (c) Dissipation for nucleation case in the simulation MIC_B1

In Figs. 14.a, b and c, the regions with dissipation $E < 0$ indicate that the nucleation of a new hydride is not favorable as the nucleating hydride should act against the hydride already present. Whereas, in the regions where $E > 0$, the hydride tends to grow easily or permit nucleation of another hydride. The dissipation maps for the cases without and with dislocation nucleation near the interface show a slight difference. In the dislocation nucleation case, the favorable hydride nucleating zone is anisotropic. In-fact, the fact that the favorable hydride nucleation zone is at an angle with respect to the horizontal plane indicates that there might be a connection to the spacing and orientation observed in the hydride stacks.

The effective shielding distance around a hydride is calculated by plotting dissipation (E) on a line parallel to the Z-axis as shown in Fig. 15a. The dissipation for the cases of hydride in Zr matrix without dislocation, with dislocations and with dislocation and nucleation are presented in Fig. 15b. In the elastic case, without the presence of dislocations in the simulation volume, the dissipation along the line indicates that there is no shielding distance around the hydride. The negative value of dissipation emphasizes that no hydride can be nucleated anywhere close by. This observation contradicts the experimentally observed hydride stacks. But, the presence of a shielding distance for both relaxation and nucleation (Fig. 15.b) cases, stresses the importance of mechanical field due to dislocations near the hydride. The effective shielding distance (dotted lines in Fig. 15.b) for the cases with and without dislocation nucleation is close to 1000a = 323nm (where a is lattice parameter) indicating the possible nucleation of another hydride very close by. These observations provide us a better understanding of hydride stacks and the local arrangement.

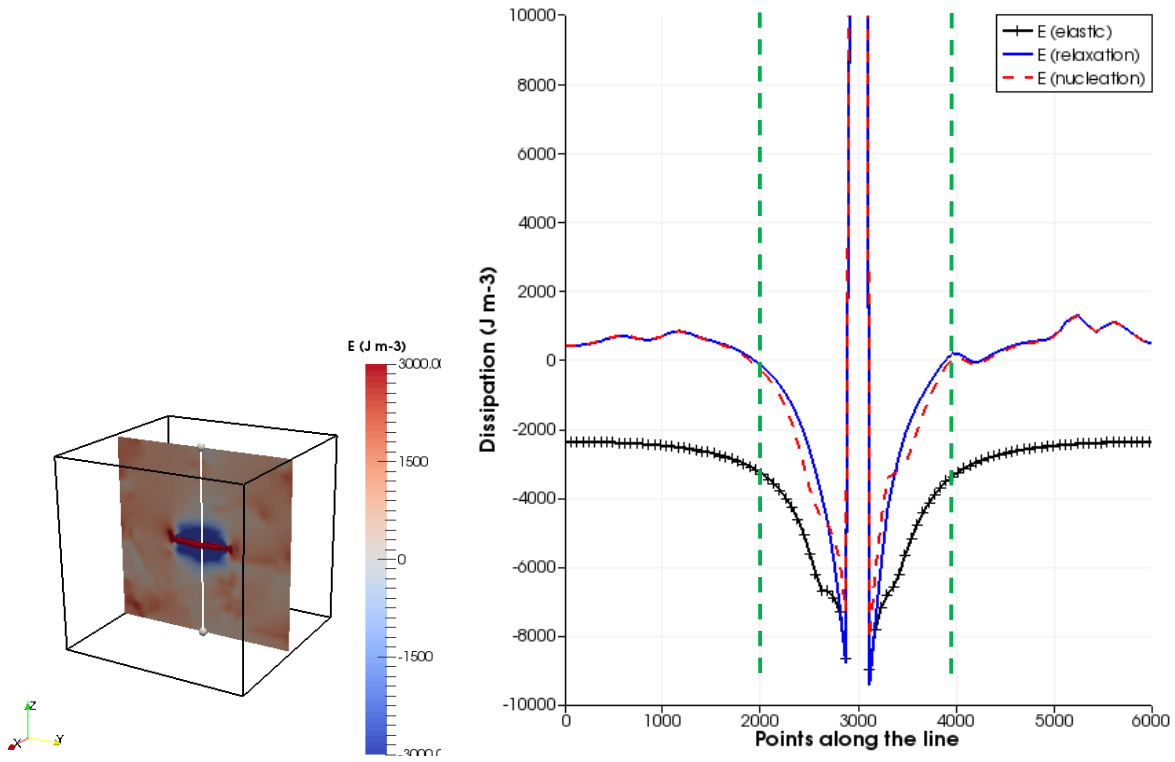

Fig. 15. (a) Line parallel to Z-axis along with dissipation is plotted; (b) Comparison of dissipation along the line shown in Fig. 15. as for the elastic, relaxation and nucleation cases in the simulation MIC_B1

5. Conclusion

In this work, a preliminary study has been performed using DDD-FFT simulations to quantify the contribution of mechanical fields on self-organization of hydride stacks. Results show a promising trend in moving ahead for better addressing the formation of hydride stacks in Zr alloys. The main conclusions drawn from the study are:

1. Plastic relaxation around a hydride was observed to be independent of total dislocation densities in Zr matrix.
2. Dislocation nucleation around the hydride had a major influence modifying the overall dissipation energy in the system. Anisotropy of dissipation energy in the case of nucleation indicates that the hydride favors growing along the direction where $E > 0$.
3. Effective shielding distance calculated was observed to be linked to the hydride largest dimension.

These results are promising and show a new perspective in our understanding of stack of hydrides in Zr. More work needs to be done with different aspect ratios and different dislocation nucleation conditions to arrive at a final conclusion on hydride stack arrangement and mechanical fields pertaining to them.

References

[1] A. Akhtar and A. Teghtsoonian, "Plastic deformation of zirconium single crystals," Acta Metallurgica, vol. 19, 1971.

[2] S. Arsene, M. Veleva, M.-C. Record, J. L. Bechade, and J. Bai, "Hydride embrittlement and irradiation effects on the hoop mechanical properties of pressurized water reactor (PWR) and boiling-water reactor (BWR) Zircaloy cladding tubes: Part II. Morphology of hydrides investigated at different magnifications and their interaction with the processes of plastic deformation," Metallurgical and Materials Transactions A, vol. 34A, 2003.

[3] B. Cox, "Hydrogen uptake during oxidation of zirconium alloys," Journal of Alloys and Compounds, vol. 256, pp. 244–246, 1997.

[4] J. E. Bailey, "Electron microscope observations on the precipitation of zirconium hydride in zirconium," Acta Metallurgica, vol. 11, 1963.

[5] K. G. Barraclough and C. J. Beevers, "Some observations on the phase transformations in zirconium hydrides," Journal of Nuclear Materials, vol. 34, pp. 125–134, 1970.

[6] A. T. W. Barrow, A. Korinek, and M. R. Daymond, "Evaluating zirconium-zirconium hydride interfacial strains by nano-beam electron diffraction," Journal of Nuclear Materials, vol. 432, no. 1-3, pp. 366– 370, 2013.

[7] N. Bertin, M. V. Upadhyay, C. Pradalier, and L. Capolungo, "A FFT-based formulation for efficient mechanical fields computation in isotropic and anisotropic periodic discrete dislocation dynamics," Modelling and Simulation in Materials Science and Engineering, vol. 23, no. 065009, 2015.

[8] I. J. Beyerlein and C. N. Tomé, "A dislocation-based constitutive law for pure Zr including temperature effects," International Journal of Plasticity, vol. 24, no. 5, pp. 867–895, 2008.

[9] M. S. Blackmur, J. D. Robson, M. Preuss, O. Zanellato, R. J. Cernik, S. Shi, F. Ribeiro, and J. Andrieux, "Zirconium hydride precipitation kinetics in Zircaloy-4 observed with synchrotron X-ray diffraction," Journal of Nuclear Materials, vol. 464, pp. 160–169, 2015. 2

[10] G. J. Carpenter, "The dilatational misfit of zirconium hydrides precipitated in zirconium," Journal of Nuclear Materials, vol. 48, pp. 264–266, 1973.

[11] G. J. Carpenter, J. F. Watters, and R. W. Gilbert, "Dislocations generated by zirconium hydride precipitates in zirconium and some of its alloys," Journal of Nuclear Materials, vol. 48, pp. 267–276, 1973.

[12] A. T. Motta and L.-Q. Chen, "Hydride Formation in Zirconium Alloys," vol. 64, no. 12,

pp. 1403–1408, 2012.

[13] H. Chung, “Proceedings in International meeting on LWR fuel performance”, USA, 2000

[14] C. E. Coleman and D. Hardie, “The hydrogen embrittlement of zirconium in slow-bend test,” Journal of Nuclear Materials, vol. 19, pp. 1–8, 1966.

[15] E. Conforto, I. Guillot, and X. Feaugas, “Solute hydrogen and hydride phase implications on the plasticity of zirconium and titanium alloys: a review and some recent advances,” Philosophical Transasctions A, vol. 375, p. 20160417, 2017.

[16] U. Dahmen, M. Witcomb, and K. Westmacott, “Aspects of faceting in the study of precipitate interfaces,” Journal de Physique Colloques, vol. 51, no. C1, pp. 737–744, 1990.

[17] C. E. Ells, “Hydride Precipitates in zirconium alloys,” Journal of Nuclear Materials, vol. 28, pp. 129–151, 1968.

[18] H. Emmerich, “Advances of and by phase-field modelling in condensed matter physics,” Advances in Physics, 2008.

[19] E. S. Fisher and C. J. Renken, “Single-Crystal Elastic Moduli and the hcp → bcc Transformation in Ti, Zr, and Hf,” Physical Review, vol. 135, no. 2A, 1964.

[20] B. Hanson, H. Alsaed, C. Stockman, D. Enos, R. Meyer, and K. Sorenson, “Gap analysis to Support extended storage of used nuclear fuel,” tech. rep., U.S. DOE, 2012. 3

[21] M. Javanbakht and V. I. Levitas, “Interaction between phase transformations and dislocations at the nanoscale. Part 2 Phase field simulation examples,” Journal of the Mechanics and Physics of Solids, vol. 82, pp. 164–185, 2015.

[22] P. A. T. Olsson, A. R. Massih, J. Blomqvist, A. A. Holston, and C. Bjerkén, “Ab initio thermodynamics of zirconium hydrides and deuterides,” Computational Materials Science, vol. 86, pp. 211–222, 2014.

[23] M. P. Puls, The Effect of Hydrogen and Hydrides on the Integrity of Zirconium Alloy Components. Springer, 2012.

[24] R. Singh, P. Stahle, L. Banks-Sills, M. Ristinmaa, and S. Banerjee, “δ-Hydride Habit Plane Determination in α-Zirconium at 298 K by Strain Energy Minimization Technique,” Defect and Diffusion Forum, vol. 279, pp. 105–110, 2008.

[25] Toshio Mura, Micromechanics of Defects in Solids. Kluwer Academic Publishers, second, re ed., 1980.